Successive bifurcations in a simple model of atmospheric zonal-flow vacillation

Seongjoon Koo and Michael Ghil
Department of Atmospheric Sciences and Institute of Geophysics and Planetary Physics, University of California, Los Angeles, Los Angeles, California 90095

(Received 10 September 2001; accepted 30 January 2002)

Low-frequency variability of the atmospheric flow in the Southern Hemisphere is dominated by irregular changes in the latitude and intensity of the mid-latitude eastward jet about its climatological mean state. This phenomenon, known as atmospheric zonal-flow vacillation, is characterized by the existence of two persistent states of the zonal (i.e., east–west oriented) jet and irregular transitions between them. Nonlinear interactions between the mean flow and the waves play a key role in the dynamics of this vacillation. In the present study, we develop a low-order, deterministic model for the nonlinear dynamics of atmospheric zonal-flow vacillation. Multiple equilibria arise in this model's zonal-mean flow, that is, in the longitudinal flow averaged along a given latitude circle. These equilibria bear a strong resemblance to the two persistent flow regimes found in Southern Hemisphere observations. The two equilibrium states are maintained by wave forcing against surface drag, as in the observations. Successive bifurcations to periodic and chaotic zonal-mean flow regimes occur as the model's dissipation parameter is reduced. © *2002 American Institute of Physics.* [DOI: 10.1063/1.1468249]

The atmosphere is a dynamical system with a very large number of degrees of freedom. It thus exhibits a vast range of spatial and temporal variability. The simplest and most fundamental mode of such variability, on the time scale of 10–100 days, is atmospheric zonal-flow vacillation. Earlier studies viewed zonal-flow vacillation as a red-noise process, driven by white-noise fluctuations in time and subject only to a linear, negative feedback. This linear stochastic framework lacks credible physics and fails to provide dynamically and statistically consistent explanations of the phenomenon. In the present work we propose a simple, nonlinear, deterministic model that captures key features of atmospheric zonal-flow vacillation, including both its morphology and its inherent dynamics.

I. INTRODUCTION

The nonlinear, deterministic dynamics of geophysical flows has been studied extensively starting with the work of Stommel,[1] Lorenz,[2] and Veronis.[3] Theoretical, experimental, and numerical studies led to a deeper understanding of the unstable and nonlinear nature of these flows. Large-scale atmospheric flows illustrate well the nonlinear workings of nature due, on the one hand, to the effects of Hamiltonian nonlinearity in the presence of small forcing and dissipation[4,5] and, on the other, to the relatively dense set of sustained observational data.[6] We focus here on the low-frequency variability (LFV) of atmospheric zonal-mean flow in mid-latitudes.

LFV refers to variability whose time scale is longer than that of major weather phenomena, i.e., longer than 5–6 days, and shorter than a season. The LFV of tropospheric mid-latitude circulation in the Southern Hemisphere contains a large zonally symmetric component, i.e., symmetric with respect to rotations about the Earth's axis.[7] The dominant mode of the observed variability of zonal-mean flow was found, using principal component analysis,[8] to have a deep annular structure, with two variability centers of opposite sign near 40 °S and 60 °S.[9] The temporal evolution of this mode is irregular, having no significant spectral peaks, and is known as atmospheric zonal-flow vacillation.[9]

Zonal-flow vacillation is characterized by the existence of two persistent zonal-jet states and irregular transitions between them. This suggests the presence of multiple flow regimes. Charney and associates[10] proposed this concept, as developed further by Reinhold and Pierrehumbert[11] and Legras and Ghil,[12] to characterize atmospheric LFV in terms of residence in and transitions between a small number of regions in phase space. In this view of LFV, the system's trajectory slows down in these regions, while the transitions among them are rather abrupt. The slowing down of the phase-space trajectory is manifested as persistent flow patterns in physical space.

The signature of the multiple flow regimes can be identified as local density maxima in a probability density function (PDF) defined on the phase space. By examining the PDFs of zonal-mean flow in Southern Hemisphere observations as well as in an atmospheric model of intermediate complexity, with about 500 degrees of freedom, Koo and colleagues[13] recently presented evidence for multiple flow regimes in atmospheric zonal-mean flow.

We study here the origin of these multiple regimes. To this end we construct in Sec. II a highly truncated version of a two-layer quasigeostrophic channel model.[4,5] The framework of hierarchical modeling—from the simplest conceptual models, through those of intermediate spatial resolution and physical detail, all the way to very detailed simulation

TABLE I. Selected meteorological terminology used in the present study.

Geostrophic balance	Momentum balance between the Coriolis force and the pressure gradient force
Potential temperature	Temperature that a parcel of dry air, at an arbitrary position, would acquire if it moved adiabatically to a reference pressure level, usually taken as 1000 hPa
Surface drag	Friction between the air flow above and Earth's surface
Vorticity	Microscopic measure of the fluid's rotation
Zonal	East–west oriented
Zonal-flow vacillation	Irregular changes in the latitude and intensity of the mid-latitudeeastward jet about its climatological mean state
Zonal mean	Average along a given latitudinal circle
Zonally symmetric	Symmetric with respect to rotations about Earth's axis

models—has become essential to understand the fundamental processes that underlie the inherently complex behavior of a large dynamical system, such as the atmosphere.[14] The horizontal truncation of our model corresponds to the lowest possible resolution that captures the zonal-flow variability associated with the vacillation.

Using this simple model we explore in Sec. III the dynamical origin of the multiple flow regimes that occur in more detailed and realistic models, as well as in the Southern Hemisphere observations. The low-order model's nonlinear behavior, including its successive bifurcations and transition to chaos,[15] is carefully examined. The underlying mechanisms that lead to this nonlinear behavior are explained and the implications of our results for the multiple flow regimes in atmospheric zonal-mean flow are discussed in Sec. IV. Concluding remarks follow in Sec. V.

II. LOW-ORDER MODEL DERIVATION

We consider a simple quasigeostrophic model of the atmosphere, i.e., a model in which the dominant balance is between the Coriolis force and the pressure gradient, modified by the nonlinear transport of vorticity by the flow itself. These models neglect motions that are faster than weather phenomena,[4,5,16] such as gravity waves or sound waves. The model domain is a mid-latitude, periodic channel centered at latitude ϕ_0. The meridional boundaries of the channel are at $y=0$ and πL, where L is a horizontal length scale. The model has two vertical layers centered at the 250 and 750 hPa pressure surfaces.

The governing equations are derived fundamentally from Newton's second law of motion and the first law of thermodynamics for a viscous fluid under the influence of gravity and rotation. The conservation of momentum subject to the quasi-geostrophic approximation can be conveniently expressed in vorticity form. The conservation of thermodynamic energy in the atmosphere can be compactly written in terms of potential temperature.

Selected meteorological terminology used in the present study is summarized in Table I, for the benefit of the interested but nonexpert reader. Further clarification can be found in a number of texts.[4,5,16]

The resulting quasigeostrophic vorticity and thermodynamic energy equations are valid on the large spatial and long time scales of interest here. We use a vertical discretization due to Lorenz,[17] to obtain the following two-layer form of these equations:

$$\frac{\partial}{\partial t}\nabla^2\psi = -J(\psi,\nabla^2\psi) - J(\tau,\nabla^2\tau) - \beta_0\frac{\partial\psi}{\partial x} - \tfrac{1}{2}k_d\nabla^2(\psi-\tau), \tag{1}$$

$$\frac{\partial}{\partial t}\nabla^2\tau = -J(\psi,\nabla^2\tau) - J(\tau,\nabla^2\psi) - \beta_0\frac{\partial\tau}{\partial x} - \frac{f_0 w}{H} + \tfrac{1}{2}k_d\nabla^2(\psi-\tau), \tag{2}$$

$$\frac{\partial\theta}{\partial t} = -J(\psi,\theta) - \frac{\sigma}{H}w + h_d'(\theta^*-\theta). \tag{3}$$

The following notation has been used.

ψ_1	upper-level streamfunction
ψ_2	lower-level streamfunction
ψ	$[=(\psi_1+\psi_2)/2]$, mean streamfunction (also called barotropic)
τ	$[(\psi_1-\psi_2)/2]$, shear streamfunction (also called baroclinic)
w	vertical velocity at the interface
θ_1	upper-level potential temperature
θ_2	lower-level potential temperature
θ	$[=(\theta_1+\theta_2)/2]$, mean potential temperature
θ^*	mean potential temperature at radiative equilibrium
H	the characteristic depth of either layer
σ	static-stability parameter
k_d	the Ekaman damping coefficient at the bottom surface
h_d'	the Newtonian cooling coefficient
f	$[f_0+\beta_0 y]$, the Coriolis parameter

Here $J(a,b)$ is the Jacobian of a and b with respect to x and y, while ∇^2 is the Laplacian.

The Coriolis parameter $f=2\Omega\sin\phi$—where Ω is the angular velocity of the Earth about its axis and ϕ the local latitude—is simplified, due to the model's flat channel geometry, by expanding it in a truncated Taylor series about the latitude ϕ_0 of the channel's center. Thus, the constant coefficient f_0 is the Coriolis parameter at latitude ϕ_0 and the so-called beta parameter β_0 is its derivative with respect to y at latitude ϕ_0. The magnitude of mechanical damping at the Earth's surface is adjusted by the coefficient k_d. The static stability parameter σ is a measure of the stability of the atmosphere in hydrostatic equilibrium with respect to vertical displacements of an air parcel.

Mid-latitude atmospheric flows are driven by quasigeostrophic response to the pole-to-equator differential in radiative heating. In our model, this thermal forcing is represented by the last term in Eq. (3). Here potential temperature is relaxed toward a given equilibrium value θ^* with a relaxational time scale given by the reciprocal of h_d'.

The system of equations is closed by the thermal-wind equation

$$\nabla^2\theta = A\nabla^2\tau, \tag{4}$$

which results from geostrophic balance and the hydrostatic approximation of no vertical acceleration that is also valid for planetary-scale flows. The constant coefficient A is defined as

$$A = \frac{2f_0}{c_p[(P_2/P_{00})^\kappa - (P_1/P_{00})^\kappa]},$$

c_p is the specific heat at constant pressure, $\kappa = R/c_p$, and R is the universal gas constant; $P_1 = 250$ hPa, $P_2 = 750$ hPa, and $P_{00} = 1000$ hPa denote pressure at the upper, lower, and surface level, respectively.

The variables are nondimensionalized as follows: y by L,x by L/n, where n is the aspect ratio of the two horizontal length scales, t by f_0^{-1}, ψ and τ by $L^2 f_0$, θ by $AL^2 f_0$, w by Hf_0, k_d and h_d' by f_0, σ by $AL^2 f_0$, and β_0 by $f_0 L^{-1}$. Our dimensionless constants are $\beta \equiv La^{-1}\cot\phi_0$, where a is the radius of the earth, $\sigma_0 \equiv \sigma(AL^2 f_0)^{-1}$, $2k \equiv k_d f_0^{-1}$, and $h'' \equiv h_d' f_0^{1-1}$; our dimensionless channel has width π and zonal length 2π.

The dependent variables are expanded in the eigenfunctions F_i of the Laplace operator,

$$\nabla^2 F_i = -a_i^2 F_i, \tag{5}$$

subject to the boundary

$$\frac{\partial F_i}{\partial x} = 0 \quad \text{at } y = 0,\pi, \tag{6}$$

and orthonormality conditions

$$\overline{F_i F_j} = \delta_{ij}, \tag{7}$$

where δ_{ij} is the Kronecker delta function and

$$\overline{(\ )} \equiv \frac{\int_0^\pi \int_0^{2\pi} (\ )\,dx\,dy}{\int_0^\pi \int_0^{2\pi} dx\,dy}.$$

We simplify the two-layer quasigeostrophic system to the utmost by retaining the fewest modes that still capture the key elements of zonal-flow vacillation. The simplest choice is to retain two y modes and one x wave.[18] This allows fluctuating zonal-mean flows in a meridional plane via the interaction between zonal-mean flow and waves that propagate in the x direction. Thus, the eigenfunctions are

$$F_1 = \sqrt{2}\cos(y), \quad F_2 = 2\cos(x)\sin(y), \tag{8}$$

$$F_3 = 2\sin(x)\sin(y),$$

$$F_4 = \sqrt{2}\cos(2y), \quad F_5 = 2\cos(x)\sin(2y), \tag{9}$$

$$F_6 = 2\sin(x)\sin(2y).$$

The expansion of the dependent variables takes the form

$$\{\psi,\tau,\theta,w\}(x,y,t) = \sum_{i=1}^{6} \{\psi_i,\tau_i,\theta_i,-\omega_i\}(t)F_i(x,y). \tag{10}$$

Following Refs. 18 and 19, the thermal forcing is represented by a single zonal component

$$\theta^*(x,y) = \theta_1^* F_1(y). \tag{11}$$

The nonlinear, conservative terms in the model equations are expanded as

$$J(F_j,F_m) = \sum_i c_{ijm}F_i, \tag{12}$$

where c_{ijm} are interaction coefficients defined by

$$c_{ijm} \equiv \overline{F_i J(F_j,F_m)}.$$

The expansion of the β term uses the relation

$$\frac{\partial F_m}{\partial x} = \sum_i b_{im}F_i, \tag{13}$$

where

$$b_{im} = \overline{F_i \frac{\partial F_m}{\partial x}}.$$

We use the thermal-wind balance (4) to replace τ with θ and thus arrive at the nondimensional, spectrally decomposed form of Eqs. (1)–(3), namely,

$$\frac{d\psi_i}{dt} = \frac{n}{2}a_i^{-2}\sum_{j=1}^{6}\sum_{m=1}^{6} c_{ijm}(a_j^2 - a_m^2)(\psi_j\psi_m + \theta_j\theta_m) + n\beta a_i^{-2}\sum_{i=1}^{6} b_{ij}\psi_j - k(\psi_i - \theta_i), \tag{14}$$

$$\frac{d\theta_i}{dt} = \frac{n}{2}a_i^{-2}\sum_{j=1}^{6}\sum_{m=1}^{6} c_{ijm}(a_j^2 - a_m^2)(\psi_j\theta_m + \theta_j\psi_m) + n\beta a_i^{-2}\sum_{i=1}^{6} b_{ij}\theta_j + k(\psi_i - \theta_i) - a_i^{-2}\omega_i, \tag{15}$$

$$\frac{d\theta_i}{dt} = -n\sum_{j=1}^{6}\sum_{m=1}^{6} c_{ijm}\psi_j\theta_m + \sigma_0\omega_i + h''(\theta_i^* - \theta_i). \tag{16}$$

One can eliminate ω_i by combining Eqs. (15) and (16). We thus obtain a system of 12 nonlinear ordinary differential equations (ODEs) for the variables $\psi_i(t)$ and $\theta_i(t)$; they are listed in full in the Appendix.

The configuration of our low-order model is somewhat similar to those of Lorenz,[18] Charney and Straus,[19] and Reinhold and Pierrehumbert.[11] There are, however, important differences. Lorenz's[18] model of 14 ODEs was constructed to simulate the flow in a thermally heated rotating tank. Our model is designed to simulate instead key features of atmospheric zonal-flow vacillation. To this end, we adopted the so-called β-plane approximation, which allows the Coriolis parameter f to vary linearly with latitude about the center of the channel,[4,5,16] rather than Lorenz's f-plane approximation, in which f is kept constant and thus Earth's sphericity is totally neglected. In rotating-tank experiments, the so-called static stability of the fluid at rest is adjusted by large-scale "sloping convection,"[20] while in the atmosphere it is primarily determined by small-scale moist convection. Thus, an equation that governs the time variation of static stability $\sigma = \sigma(t)$ in the Lorenz model[18] has been dropped. Instead, this quantity is held constant in our model, as in other dry quasigeostrophic models of the atmosphere.

Unlike in the models of Refs. 11 and 19, there is no topography in our model. Thus, our model's waves are not externally forced through topographic resonance.[4,10] Our model's horizontal resolution follows Lorenz[18] and differs from that of Refs. 11 and 19.

III. SUCCESSIVE BIFURCATIONS AND TRANSITION TO CHAOS

We present stationary and time-dependent solutions of our low-order model [Eqs. (A1)–(A12)], in a range of parameter values that are close to Earthlike settings. The scaling constants are set as follows: $\phi_0 = 45\,^\circ\mathrm{N}$, $L = 1600$ km, $a_0 = 6400$ km, $H = 7.5$ km, $f_0 = 1 \times 10^{-4}\ \mathrm{s}^{-1}$, and $A = 8.03 \times 10^{-7}\ \mathrm{s\,K\,m}^{-2}$. Nondimensional parameter values are chosen as follows: $\beta = 0.25$, $\sigma_0 = 0.15$, $\theta_1^* = 0.105$, $n = 1.5$, while the control parameter $k = h''$ is allowed to range over the interval [0.047, 0.120]. With this choice of L and n, the channel has a width of $\pi L = 5027$ km and a length of $2\pi L/n = 6702$ km. This is approximately the size of the North or South Atlantic basin.

The thermal forcing parameter θ_1^* is associated in our model with the temperature change, at radiative equilibrium, across the channel's midlevel through the relation

$$\Delta T^* = \left(\frac{4\sqrt{2} L^2 f_0^2}{R} \right) \theta_1^* . \tag{17}$$

The choice of $\theta_1^* = 0.105$ is equivalent to $\Delta T^* = 53.0$ K. This is in rough agreement with observations. Note that our thermal forcing is much weaker than that of Lorenz[18] or Charney and Straus.[19] Other parameter values are within the ranges of Earthlike settings given by Ref. 11.

We explore solution behavior by changing the dissipation parameter k and study successive bifurcations of the system, from the most stable flow regime to the most unstable one.[4,6,15,21] To do so, we first solve the model analytically for the simplest flow regime, the steady Hadley circulation, in which no wave components appear. We note that if all the wave components (i.e., the variables with subscripts 2, 3, 5, and 6) in Eqs. (A1)–(A12) vanish identically, the equations that govern these variables are automatically satisfied. In this case, the equations that govern ψ_4 and θ_4 indicate that these variables also vanish.

Thus, the entire set of ODEs is reduced to the two equations for ψ_1 and θ_1. The resulting steady-state solution is

$$\psi_1 = \theta_1 = \theta_1^* . \tag{18}$$

We call this unique stationary solution the *Hadley solution*, following Ref. 18, because it corresponds to the zonally symmetric Hadley cell on Earth.[4] Note that no multiple equilibria of purely zonal flow are possible.

Next, we seek time-dependent solutions by numerical integration of the model [Eqs. (A1)–(A12)]. Our system of ODEs is not stiff and can thus be solved accurately by using an explicit Runge–Kutta (4,5) formula, the Dormand–Prince pair.[22] The numerical scheme is adaptive, that is, the integration time step is automatically decreased to reach the desired accuracy. We use a relative and an absolute tolerance of 10^{-10}. All time integrations are conducted for 50 000 nondimensional time units, i.e., an interval equivalent to 5833 days, and results are saved every 1.0 nondimensional time unit. The model integrations start with an initial state of weak wave perturbations, $\psi_2 = \psi_6 = 1.0 \times 10^{-3}$. All other components are initially set to zero.

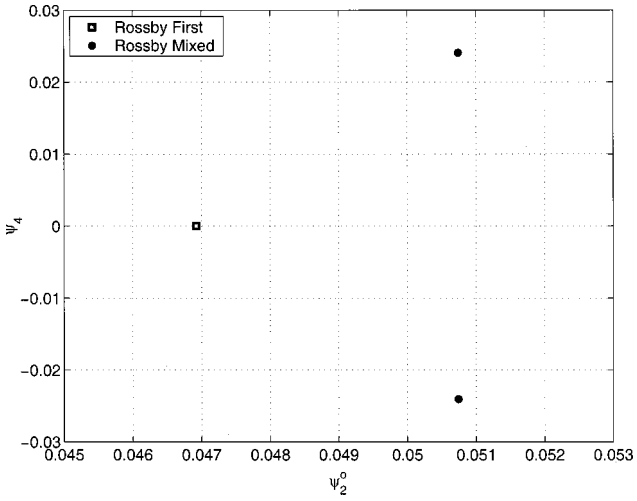

FIG. 1. Projection of phase-space trajectories on the plane of ψ_2^0 and ψ_4 for the first Rossby mode ($k = 0.09$) and the Rossby mixed mode ($k = 0.068$); ψ_2^0 is the ''frozen'' coefficient of the first-mode wave (see text for details).

For the control parameter value of $k = 0.12$, the numerical solution (not shown) exhibits a steady Hadley circulation that is identical to the analytical solution. This circulation becomes unstable when k is decreased and it undergoes a Hopf bifurcation.[4,21] As a result, the first wave components ψ_2 and ψ_3 attain self-sustained oscillations with constant amplitudes. We call this new flow regime, following Ref. 18, the first Rossby mode, since it exhibits certain properties of the midlatitude Rossby waves on Earth.[4,5,16] The projection of the corresponding limit cycle onto a plane is shown in Fig. 1 for $k = 0.09$. The unique period associated with this regime equals 20.5 days.

The first Rossby mode becomes unstable to perturbations in the second y mode as the dissipation parameter k is reduced further. As a result, the wave components associated with the second y mode reach self-sustained oscillations, in addition to those already present in the first wave components. The new flow regime, characterized by coexisting waves of the first and second y mode, is named the Rossby mixed mode, as in Ref. 18. A projection of the limit cycle associated with the Rossby mixed mode at $k = 0.068$ is also shown in Fig. 1. The stable period attained in this case equals 22.8 days.

Both the Rossby first- and mixed-mode solutions have propagating wave components. As shown by Lorenz,[18] these waves can be ''frozen'' by choosing a frame of reference that travels along at the wave speed. The ''freezing of the waves'' corresponds to the following change of variables:

$$\psi_2^0 = \sqrt{\psi_2 \psi_2 + \psi_3 \psi_3}, \quad \psi_3^0 = 0, \tag{19}$$

$$\psi_5^0 = (\psi_2 \psi_5 + \psi_3 \psi_6) / \sqrt{\psi_2 \psi_2 + \psi_3 \psi_3},$$
$$\psi_6^0 = (\psi_2 \psi_6 - \psi_3 \psi_5) / \sqrt{\psi_2 \psi_2 + \psi_3 \psi_3}, \tag{20}$$

$$\theta_2^0=(\psi_2\theta_2+\psi_3\theta_3)/\sqrt{\psi_2\psi_2+\psi_3\psi_3},$$
$$\theta_3^0=(\psi_2\theta_3-\psi_3\theta_2)/\sqrt{\psi_2\psi_2+\psi_3\psi_3}, \quad (21)$$
$$\theta_5^0=(\psi_2\theta_5+\psi_3\theta_6)/\sqrt{\psi_2\psi_2+\psi_3\psi_3},$$
$$\theta_6^0=(\psi_2\theta_6-\psi_3\theta_5)/\sqrt{\psi_2\psi_2/\psi_3\psi_3}. \quad (22)$$

This physically motivated, time-dependent change of coordinates corresponds to the mathematical device of ''freezing coefficients'' in Floquet theory (see Sec. 5.3 in Ref. 4 and also Ref. 23).

In spite of the periodic wave motion, the Rossby mixed-mode solutions' zonal-mean components ψ_1 and ψ_4 reach steady states, with nonzero ψ_4. This results in a steady zonal-mean flow

$$U(y)=\sqrt{2}\psi_1\sin(y)+2\sqrt{2}\psi_4\sin(2y), \quad (23)$$

whose jet maximum is shifted away from the channel center. The Rossby mixed mode has another stable solution with the sign of ψ_4 reversed when the sign of the ψ_2 or ψ_6 perturbation in the initial state is reversed (see also Fig. 1). Therefore, there exist two distinct stable circulations of the Rossby mixed mode. The multiple equilibria in zonal-mean flow are characterized by the two steady zonal jet states, whose jet maximum is located away from the channel center either on the poleward or equatorward side.

The Rossby mixed-mode regime becomes unstable and another stable flow regime appears as the control parameter k is reduced further. This regime is characterized by zonal-mean flows that oscillate around the Rossby mixed-mode solutions. We call this new flow regime unsymmetric vacillation. In this regime, unlike for the first-mode and mixed-mode regime, the wave components ψ_2, ψ_3, ψ_5, and ψ_6 contain more than one oscillatory mode. For example, the power spectra for the unsymmetric vacillation with $k=0.0608$ reveals three oscillatory modes with period 21.3, 28.7, and 163.8 days, as well as harmonics of the two short-period oscillations (not shown).

The zonal-mean components, ψ_1 and ψ_4, also exhibit anharmonic oscillations, whose shape differs markedly from a sinusoid. For $k=0.0608$, for example, power spectra indicate that these highly nonlinear oscillations are composed of the fundamental oscillatory mode with period 24.5 days and its harmonics. As in the case of the Rossby mixed mode, there is another stable flow regime, with the sign of ψ_4 reversed. Either of the multiple zonal-mean flow solutions is realized depending upon the initial state.

When the control parameter k is reduced even further a chaotic[24] flow regime appears. In this regime, all the zonal-mean and wave components exhibit aperiodic, irregular signals. Our model's irregular flows exhibit sensitivity to initial data, a typical sign of deterministic chaos, as illustrated in Fig. 2. Two initially very close trajectories that started near the origin of the (ψ_1,ψ_4) plane eventually diverge dramatically and lose their initial similarities. Even in the chaotic flow regime, two subregimes co-exist for the same parameter values: they are characterized by opposite signs of ψ_4.

The transition to chaos is further examined in Fig. 3 by projecting the model's trajectories on the plane of ψ_1 and ψ_4. Note that ψ_1 and ψ_4 fully determine the zonal-mean flow [see Eq. (23)]. For $k=0.0608$, the zonal-mean flow is purely periodic, but a small fold appears in the projection. For $k=0.0603$, a second fold in the system's trajectory corresponds to a period-doubling bifurcation. Another period-doubling bifurcation is visible for $k=0.059\,82$. Due to this

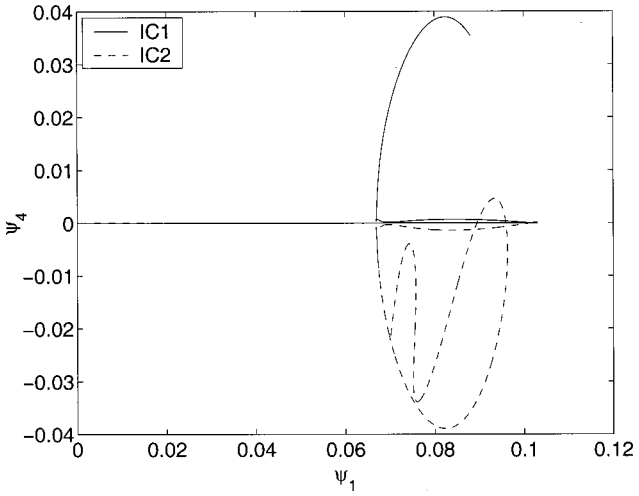

FIG. 2. Sensitivity to initial data: two trajectories (solid and dashed) with slightly different initial states (IC1 and IC2) for $k=0.055$. The trajectories are displayed on the plane spanned by ψ_1 and ψ_4 for the nondimensional time interval $0\leqslant t\leqslant 1200$.

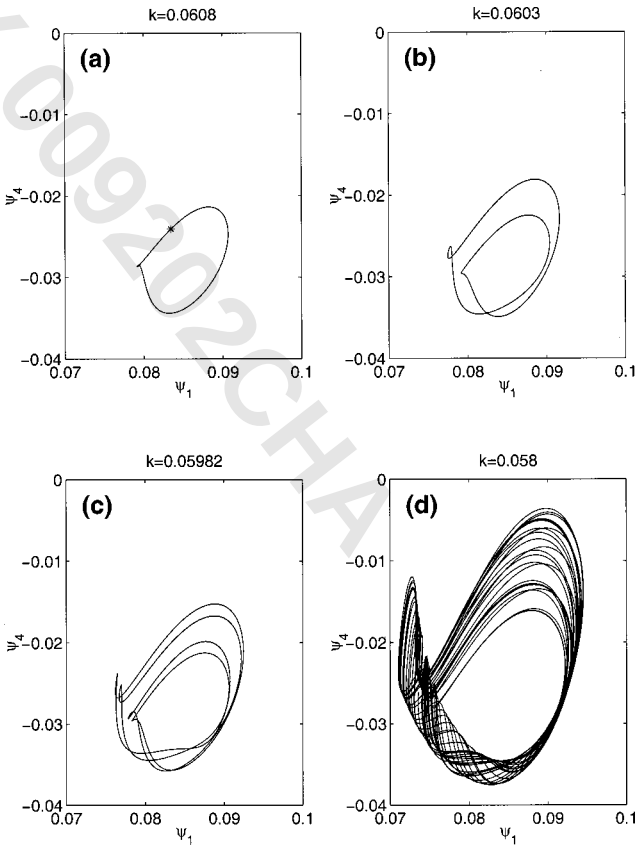

FIG. 3. Trajectories in phase space projected on the (ψ_1,ψ_4) plane for nondimensional time $t\in[3000,10000]$: (a) $k=0.0608$, (b) $k=0.0603$, (c) $k=0.05982$, and (d) $k=0.058$. The steady zonal-mean flow for $k=0.068$ is denoted by an asterisk in (a).

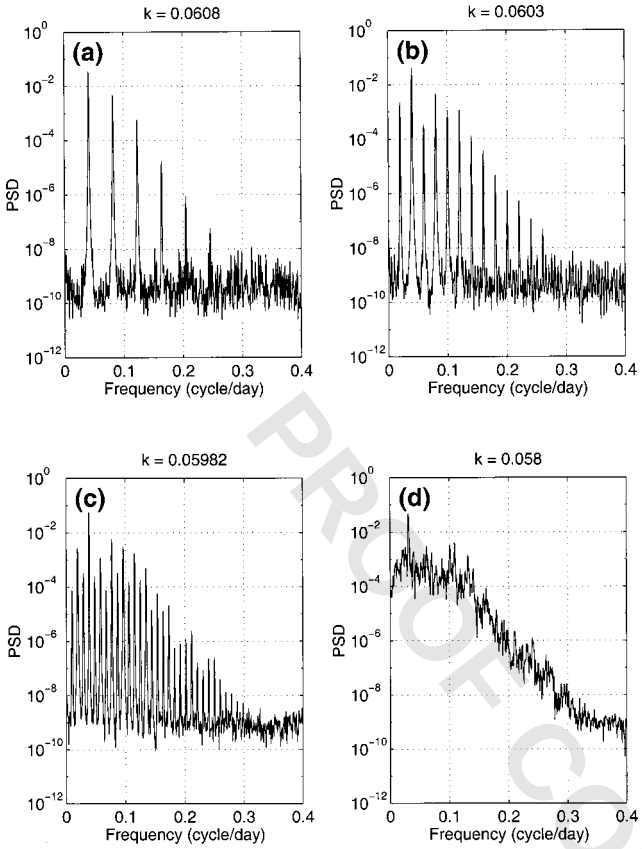

FIG. 4. Power spectra of ψ_4 for (a) $k=0.0608$, (b) $k=0.0603$, (c) $k=0.05982$, and (d) $k=0.058$.

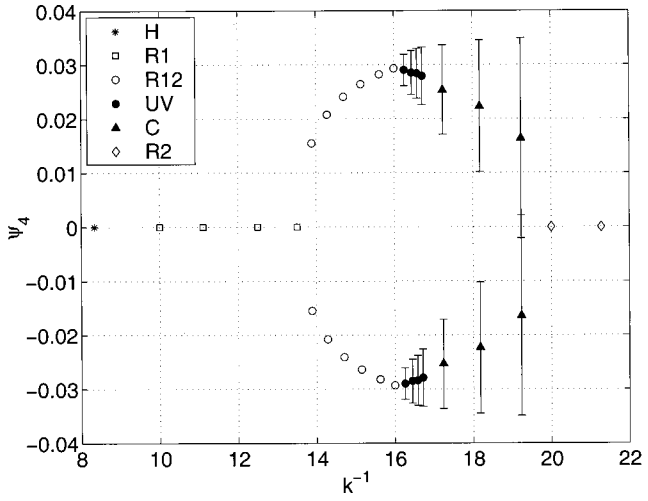

FIG. 5. Bifurcation diagram showing successive bifurcations. Six different regimes are denoted by **H** (Hadley), **R1**, (Rossby first mode), **R12** (Rossby mixed mode), **UV** (Unsymmetric Vacillation), **C** (Chaos), and **R2** (Rossby second mode) in the legend.

subharmonic cascade,[25] the system becomes chaotic for $k=0.058$. Its trajectory is somewhat reminiscent of the Rössler attractor[26] and exhibits signs of folding and stretching associated with deterministic chaos. Note that the trajectories occupy a larger portion of phase space as k becomes smaller, due to the flow's increased instability.

Figure 4 shows the power spectra of ψ_4 for the same parameter values as in Figs. 3(a)–3(d). For $k=0.0608$ several sharp spectral peaks are detected, all other peaks being harmonics of the largest peak. The fundamental frequency is $\nu_0=0.0409$ cycle/day and the corresponding period is 24.5 days. For $k=0.0603$ many other spectral peaks appear in addition to the peaks in panel (a). These additional peaks are found to be the first subharmonic of ν_0, i.e., $\nu_0/2$, and its odd multiples. Thus, the folding of the trajectories that characterizes the transition from Figs. 3(a) and 3(b) is due indeed to period doubling.

Similarly, the added peaks in panel (c) are found to be the first subharmonic of $\nu_0/2$, i.e., $\nu_0/4$, and its odd multiples. This indicates that the transition from Fig. 3(b) to 3(c) is due to another subharmonic bifurcation. For $k=0.058$, a continuous broad-band spectrum suddenly rises from 10^{-9} to 10^{-4}, while the fundamental peak at ν_0 is still visible. This manifestation of chaos detected by the spectral analysis is consistent with the irregular appearance of the phase-space trajectory in Fig. 3(d).

The successive bifurcations studied here are summarized in Fig. 5, which shows six distinctive regimes with respect to the changes in the dissipation parameter k. The vertical bars in Fig. 5 indicate $\pm$ (one standard deviation) of the variability in ψ_4. The location of a symbol within the bar denotes the variability's mean value. The corresponding bifurcation diagram for Lorenz's[18] model is shown as Fig. 5.8 in Ghil and Childress.[4]

The system first undergoes a Hopf bifurcation from the Hadley regime to the first-mode Rossby regime. The period of the oscillatory instability that gives rise to this bifurcation is intraseasonal, of the order of 20–30 days. Both regimes have $\psi_4=0$ so that the zonal-mean flow is symmetric with respect to the channel's center line. A transition from the first-mode to the mixed-mode regime then takes place and a pair of nonzero ψ_4 values appears. The Rossby mixed mode is marked by multiple equilibria in zonal-mean flow, which give the two branches in Fig. 5. The zonal-mean flow profile that corresponds to either of the two Rossby mixed-mode solutions exhibits symmetry breaking—a typical indication of nonlinearity in action—and its maximum is shifted away from the axis of the channel. The period of the mixed-mode solution is still intraseasonal.

The Rossby mixed mode's mean flow starts to oscillate due to a secondary Hopf bifurcation,[21] which leads to the unsymmetric vacillation. The period of the associated oscillatory instability is much longer, of the order of 10^2 days. The unsymmetric vacillation exists within a relatively narrow range of the control parameter values, after which a sharp transition to the chaotic regime occurs. Note that, as the control parameter k decreases further, the positive and negative ψ_4 solutions, which are solely determined by the initial state, start to overlap. This overlap between solutions becomes larger as k decreases. Further decrease in k leads to the collapse of the two solutions with opposite signs of ψ_4, which leads to the Rossby regime of the second mode.

This new regime is characterized by self-sustained oscillations in the wave components ψ_5 and ψ_6 that are associated with the second y mode. The zonal-mean flow of the Rossby second mode is symmetric with respect to the channel's cen-

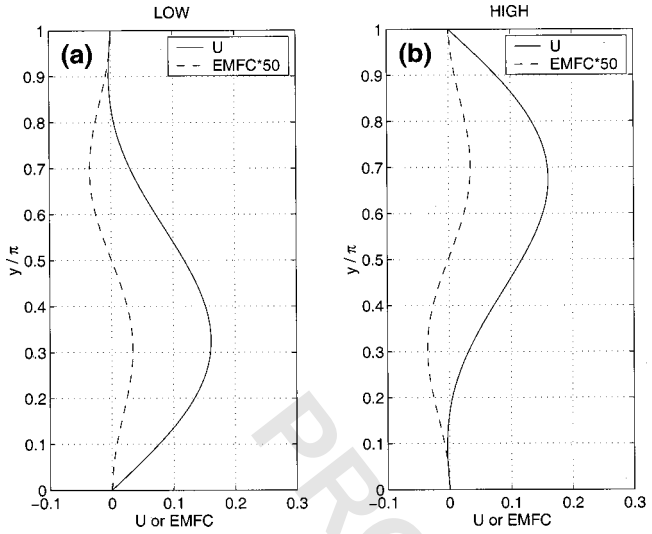

FIG. 6. Multiple equilibria in zonal-mean flow for the mixed-mode solutions obtained at $k=0.068$: (a) the low-latitude equilibrium profile; and (b) the high-latitude equilibrium profile. Solid lines indicate zonal-mean zonal flow and dashed ones denote eddy momentum flux convergence.

ter line because $\psi_4=0$ and does not have multiple values. The recovery of stability in this last transition is not physical and is probably due to the model's extreme truncation; see the discussion in Chap. 5 of Ref. 4 of the Lorenz[18] results.

IV. IMPLICATIONS FOR MULTIPLE REGIMES IN ZONAL-MEAN FLOW

We now examine the dynamics of our low-order model in physical space. As discussed in the preceding section, for the control parameter value $k=0.068$ the system has two distinct solutions with steady zonal-mean flow and propagating Rossby waves of both the first and second mode. Note that the Rossby mixed-mode solutions are thus overall periodic.

The two distinct flow regimes are shown in terms of their zonal-mean zonal flow and eddy momentum flux convergence in Fig. 6. One is characterized by the zonal-mean flow's maximum being shifted equatorward from the channel center and the other is marked by the poleward shift of this maximum. Both zonal-mean flow regimes are maintained against frictional dissipation at the bottom by the corresponding eddy momentum forcing's being in phase with the zonal-jet shift. This momentum balance is consistent with the dynamics of the two zonal-mean flow regimes, as analyzed in a more realistic primitive-equation (PE) model with much higher horizontal resolution, as well as in the Southern Hemisphere observations.[13] The PE model is derived from the full equations for the fluid's conservation of mass, momentum, and internal energy, using only the hydrostatic approximation of negligible vertical acceleration.[16,27]

The zonal-mean flow's variability in the present low-order model and its dynamics in the chaotic regime are examined next. Figure 7(a) shows a time series of ψ_4 for $k=0.052$ and indicates chaotic fluctuations of zonal-mean flow in the meridional direction. In order to study three distinct dynamical states of zonal-mean flow, we then select states with ψ_4 being negative, zero, and positive from the time series. These three states are denoted by an asterisk in Fig. 7(a).

The remaining panels in Fig. 7 show the barotropic streamfunction ψ, zonal-mean flow, and eddy momentum flux convergence for the three states. As in Fig. 6, the low- and high-latitude states are characterized by the position of the zonal-jet maximum and are sustained by the corresponding eddy momentum forcing. Consistent with this eddy momentum flux convergence, the streamfunction ψ shows two distinct tilts in the ridges and troughs of the waves: NE–SW for the high-latitude state and NW–SE for the low-latitude state.

On the other hand, the intermediate state with $\psi_4\approx 0$ shows the zonal-mean flow maximum occurring at the channel center. Its barotropic streamfunction ψ has no tilt away from the meridional direction in the waves' ridges and troughs. This is consistent with the convergence of the eddy momentum flux being almost identically zero. From the present analysis it is clear that the eddies are driving the zonal-mean flow variability, consistent with the findings of Koo and colleagues[13] in their PE model and the Southern Hemisphere observations.

Within its Earthlike parameter ranges, our low-order model represents some key elements of the dynamics of zonal-mean flow in the Southern Hemisphere, despite its drastic truncation. These striking similarities strongly suggest that the two equilibria of zonal-mean flow in our low-order model may capture the origin of the quasistationary and persistent zonal-flow regimes in the atmosphere. The chaotic regimes arising via successive bifurcations in the low-order model represent, with a certain degree of realism, the eddy-driven nature of zonal-mean flow variability in the Southern Hemisphere.

V. CONCLUDING REMARKS

We constructed a highly truncated, two-layer, quasi-geostrophic channel model in order to investigate the origin of zonal-flow vacillation in the Southern Hemisphere observations[7,9] as well as in a two-layer PE model with intermediate resolution.[13] A distinctive feature of our low-order model is that it has a flat bottom, while the role of topography has been emphasized in low-order models used in a number of previous studies that addressed Northern Hemisphere LFV.[10–12,19,28] The main LFV mechanism present in these models was the effect of topography modulating the interaction between the zonal-mean flow and equivalent-barotropic waves, whose horizontal structure does not change with height.[10,12,28] This mechanism was also found and analyzed in a laboratory setting.[29]

Multiple flow equilibria were identified in the zonal-mean flow of our low-order model (Fig. 1). They bear a strong resemblance to the two persistent flow regimes found by Koo and colleagues[13] in the Southern Hemisphere observations and in their PE model (Fig. 6). The two stationary zonal-mean flow solutions are sustained here by the wave forcing, as they are in the multiple regimes identified in the Southern Hemisphere observations and in the PE model. The

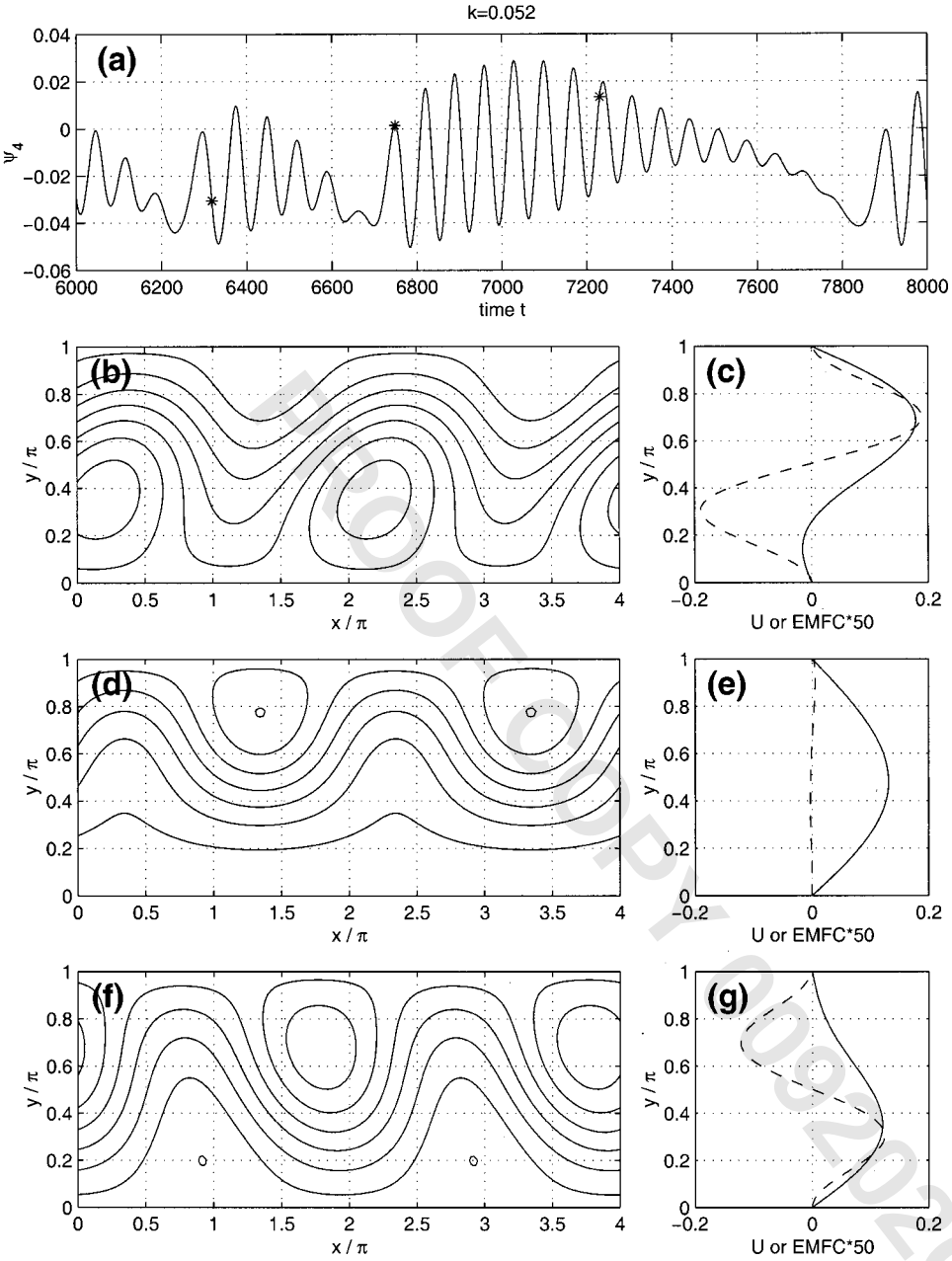

FIG. 7. Dynamical variables in physical space for the chaotic regime obtained at $k=0.052$: (a) time series of ψ_4 on which three distinct states—$\psi_4<0$, $\psi_4\approx 0$, and $\psi_4>0$—are denoted each by an asterisk; (b) barotropic streamfunction and (c) zonal-mean zonal flow (solid) and eddy momentum flux convergence (dashed) for the high-latitude state; (d) and (e) are the same as (b) and (c) but for the intermediate state; (f) and (g) are the same as (b) and (c) but for the low-latitude state.

parameter values that give rise to the multiple flow equilibria are found to be within the range of Earthlike settings. Thus, our low-order model without topography exhibits multiple equilibria that bear a strong resemblance to these persistent flow regimes in terms of morphology as well as inherent dynamics.

Successive bifurcations to periodic and irregular zonal-mean flow regimes occur as the control parameter changes. Multiple solutions that resemble the two extreme phases of zonal-flow vacillation exist in a wide range of the control parameter values (Fig. 5). Nonlinear interactions between the model's zonal-mean flow and its baroclinic waves are responsible for the chaotic variations of zonal-mean flow in the irregular flow regime (Fig. 7). Our results thus emphasize the role of vertically sheared, baroclinic waves in the Southern Hemisphere's LFV. Such baroclinic waves are known to dominate weather phenomena in both hemispheres but their role in Northern Hemisphere LFV has been less well established.[11,19,30]

As is often the case, the irregular character of time series associated with the position and intensity of the zonal jet in the Southern Hemisphere has prompted the formulation of a red-noise model of zonal-flow vacillation.[31] In such first-order Markov models, zonal-mean flow variability is explained by white-noise fluctuations in time, subject to a linear, negative feedback. This linear stochastic framework clearly lacks credible physics and fails to provide dynamically and statistically consistent explanations of the phenomenon.

In contrast to such linear stochastic models, Koo and co-authors[13] recently presented a nonlinear framework of zonal-flow vacillation, based on the paradigm of multiple flow regimes.[4,6] They presented evidence for multiple flow regimes associated with the two extreme phases of zonal-

flow vacillation in Southern Hemisphere observations, where the role of topography is much less prominent than in the Northern Hemisphere,[32] and in their deterministic, two-layer PE model, where there was no topography at all. In particular, notable asymmetries with respect to the time-mean state are present in the two regimes: they are associated with large excursions of the jet and transitions from the one to the other tend to avoid the mean rather than favor it. Unlike the linear Markov models, the perspective of multiple regimes provides a fairly complete and convincing dynamical description of atmospheric zonal-flow vacillation that is consistent with the statistical evidence. Moreover, this dynamical description is also consistent with previous studies of the dynamics of zonal-flow vacillation.[9,33]

Clearly the multiple regimes found in the Southern Hemisphere observations and in the PE model with no topography cannot be explained by the previous theories of multiple flow equilibria in the Northern Hemisphere, which emphasize the role of topography (see Refs. 9, 32, 33). Our low-order model's multiple regimes present a striking resemblance, in terms of their morphology as well as dynamics, to the regimes found in the Southern Hemisphere observations and in our PE model of intermediate complexity.[13] The explanation of the multiple regimes in atmospheric zonal-mean flow must lie, therefore, in the nonlinear baroclinic processes captured by our low-order model without topography.

Our findings suggest that nonlinearity plays a key role in the most fundamental and simplest mid-latitude LFV mode, the zonally symmetric mode. The relevance of these results to Northern Hemisphere LFV as well is still a matter of considerable debate.[6,34]

ACKNOWLEDGMENTS

It is a pleasure to thank A. W. Robertson for many useful discussions. This research was supported by NSF Grant ATM 00-82131 (M.G.), NASA Grant NAG5-7294 (M.G.), and a Chancellor's Dissertation Year Fellowship at the University of California, Los Angeles (S.K.). This is publication no. 5728 of UCLA's Institute of Geophysics and Planetary Physics.

APPENDIX: GOVERNING EQUATIONS OF THE LOW-ORDER MODEL

$$\frac{\partial \psi_1}{\partial t} = -k(\psi_1 - \theta_1), \tag{A1}$$

$$\frac{\partial \psi_2}{\partial t} = -C_2 \frac{n^3}{n^2+1}(\psi_1\psi_3 + \theta_1\theta_3) - C_4 \frac{n^3}{n^2+1}(\psi_4\psi_6 + \theta_4\theta_6) + \frac{n}{n^2+1}\beta\psi_3 - k(\psi_2 - \theta_2), \tag{A2}$$

$$\frac{\partial \psi_3}{\partial t} = C_2 \frac{n^3}{n^2+1}(\psi_1\psi_2 + \theta_1\theta_2) + C_4 \frac{n^3}{n^2+1}(\psi_4\psi_5 + \theta_4\theta_5) - \frac{n}{n^2+1}\beta\psi_2 - k(\psi_3 - \theta_3), \tag{A3}$$

$$\frac{\partial \psi_4}{\partial t} = C_3 n(\psi_2\psi_6 + \theta_2\theta_6) - C_3 n(\psi_3\psi_5 + \theta_3\theta_5) - k(\psi_4 - \theta_4), \tag{A4}$$

$$\frac{\partial \psi_5}{\partial t} = -C_1 \frac{n(n^2+3)}{n^2+4}(\psi_1\psi_6 + \theta_1\theta_6) - C_4 \frac{n(n^2-3)}{n^2+4} \times (\psi_3\psi_4 + \theta_3\theta_4) + \frac{n}{n^2+4}\beta\psi_6 - k(\psi_5 - \theta_5), \tag{A5}$$

$$\frac{\partial \psi_6}{\partial t} = C_1 \frac{n(n^2+3)}{n^2+4}(\psi_1\psi_5 + \theta_1\theta_5) + C_4 \frac{n(n^2-3)}{n^2+4} \times (\psi_2\psi_4 + \theta_2\theta_4) - \frac{n}{n^2+4}\beta\psi_5 - k(\psi_6 - \theta_6), \tag{A6}$$

$$(1+\sigma_0)\frac{\partial \theta_1}{\partial t} = C_2 n(\psi_2\theta_3 - \psi_3\theta_2) + C_1 n(\psi_5\theta_6 - \psi_6\theta_5) + \sigma_0\kappa(\psi_1 - \theta_1) + h''(\theta_1^* - \theta_1), \tag{A7}$$

$$\left(\sigma_0 + \frac{1}{n^2+1}\right)\frac{\partial \theta_2}{\partial t} = -\frac{\sigma_0 C_2 n^3}{n^2+1}(\psi_1\theta_3 + \psi_3\theta_1) - \frac{\sigma_0 C_4 n^3}{n^2+1}(\psi_4\theta_6 + \psi_6\theta_4) - \frac{C_2 n}{n^2+1}(\psi_1\theta_3 - \psi_3\theta_1) - \frac{C_4 n}{n^2+1}(\psi_4\theta_6 - \psi_6\theta_4) + \frac{\sigma_0\beta n}{n^2+1}\theta_3 + \sigma_0 k(\psi_2 - \theta_2) - \frac{h''}{n^2+1}\theta_2, \tag{A8}$$

$$\left(\sigma_0 + \frac{1}{n^2+1}\right)\frac{\partial \theta_3}{\partial t} = \frac{\sigma_0 C_2 n^3}{n^2+1}(\psi_1\theta_2 + \psi_2\theta^1) + \frac{\sigma_0 C_4 n^3}{n^2+1}(\psi_4\theta_5 + \psi_5\theta_4) + \frac{C_2 n}{n^2+1}(\psi_1\theta_2 - \psi_2\theta_1) + \frac{C_4 n}{n^2+1}(\psi_4\theta_5 - \psi_5\theta_4) - \frac{\sigma_0\beta n}{n^2+1}\theta_2 + \sigma_0 k(\psi_3 - \theta_3) - \frac{h''}{n^2+1}\theta_3, \tag{A9}$$

$$\left(\sigma_0 + \frac{1}{4}\right)\frac{\partial \theta_4}{\partial t} = \sigma_0 C_3 n(\psi_2\theta_6 + \psi_6\theta_2) - \sigma_0 C_3 n(\psi_3\theta_5 + \psi_5\theta_3) + \frac{C_4 n}{4}(\psi_2\theta_6 - \psi_6\theta_2) - \frac{C_4 n}{4}(\psi_3\theta_5 - \psi_5\theta_3) + \sigma_0 k(\psi_4 - \theta_4) - \frac{h''}{4}\theta_4, \tag{A10}$$

$$\left(\sigma_0+\frac{1}{n^2+4}\right)\frac{\partial\theta_5}{\partial t}$$
$$=-\frac{\sigma_0 C_1 n(n^2+3)}{n^2+4}(\psi_1\theta_6+\psi_6\theta_1)-\frac{\sigma_0 C_4 n(n^2-3)}{n^2+4}$$
$$\times(\psi_3\theta_4+\psi_4\theta_3)-\frac{C_1 n}{n^2+4}(\psi_1\theta_6-\psi_6\theta_1)$$
$$+\frac{C_4 n}{n^2+4}(\psi_3\theta_4-\psi_4\theta_3)+\frac{\sigma_0\beta n}{n^2+4}\theta_6$$
$$+\sigma_0 k(\psi_5-\theta_5)-\frac{h''}{n^2+4}\theta_5, \tag{A11}$$

$$\left(\sigma_0+\frac{1}{n^2+4}\right)\frac{\partial\theta_6}{\partial t}$$
$$=\frac{\sigma_0 C_1 n(n^2+3)}{n^2+4}(\psi_1\theta_5+\psi_5\theta_1)+\frac{\sigma_0 C_4 n(n^2-3)}{n^2+4}$$
$$\times(\psi_2\theta_4+\psi_4\theta_2)+\frac{C_1 n}{n^2+4}(\psi_1\theta_5-\psi_5\theta_1)$$
$$-\frac{C_4 n}{n^2+4}(\psi_2\theta_4-\psi_4\theta_2)-\frac{\sigma_0\beta n}{n^2+4}\theta_5+\sigma_0 k(\psi_6-\theta_6)$$
$$-\frac{h''}{n^2+4}\theta_6, \tag{A12}$$

where

$$\frac{C_1}{4}=\frac{C_2}{5}=\frac{C_3}{6}=\frac{C_4}{8}=\frac{8\sqrt{2}}{15\pi}.$$

[1] H. Stommel, Tellus **13**, 224 (1961).
[2] E. N. Lorenz, J. Atmos. Sci. **20**, 130 (1963).
[3] G. Veronis, J. Atmos. Sci. **20**, 577 (1963).
[4] M. Ghil and S. Childress, *Topics in Geophysical Fluid Dynamics: Atmospheric Dynamics, Dynamo Theory, and Climate Dynamics* (Springer-Verlag, New York, 1987).
[5] R. Salmon, *Lectures on Geophysical Fluid Dynamics* (Oxford University Press, New York, 1998).
[6] M. Ghil and A. W. Robertson, Proc. Natl. Acad. Sci. U.S.A. (in press).
[7] J. W. Kidson, J. Clim. **1**, 1177 (1988); **4**, 939 (1991);
[8] I. T. Jolliffe, *Principal Component Analysis* (Springer-Verlag, New York, 1986); R. W. Preisendorfer, *Principal Component Analysis in Meteorology and Oceanography* (Elsevier, New York, 1988).
[9] D. L. Hartmann and F. Lo, J. Atmos. Sci. **55**, 1303 (1998).
[10] J. G. Charney and J. G. DeVore, J. Atmos. Sci. **36**, 1205 (1979); J. G. Charney, J. Shukla, and K. C. Mo, *ibid.* **38**, 762 (1981).
[11] B. B. Reinhold and R. T. Pierrehumbert, Mon. Weather Rev. **110**, 1105 (1982); **113**, 2055 (1985).
[12] B. Legras and M. Ghil, in *Predictability of Fluid Motions*, edited by G. Holloway and B. J. West (American Institute of Physics, New York, 1984); J. Atmos. Sci. **42**, 433 (1985).
[13] S. Koo, Ph.D. thesis, University of California, Los Angeles, 2001; S. Koo, A. W. Robertson, and M. Ghil (unpublished).
[14] M. Ghil and A. W. Robertson, in *General Circulation Model Development: Past, Present, and Future*, edited by D. A. Randall (Academic, San Diego, 2000).
[15] *Hydrodynamic Instabilities and the Transition to Turbulence*, edited by H. L. Swinney and J. P. Gollub (Springer-Verlag, New York, 1981).
[16] A. E. Gill, *Atmosphere-Ocean Dynamics* (Academic, New York, 1982); J. Pedlosky, *Geophysical Fluid Dynamics* (Springer-Verlag, New York, 1987); J. R. Holton, *An Introduction to Dynamic Meteorology* (Academic, San Diego, 1992).
[17] E. N. Lorenz, Tellus **12**, 364 (1960).
[18] E. N. Lorenz, J. Atmos. Sci. **20**, 448 (1963).
[19] J. G. Charney and D. M. Straus, J. Atmos. Sci. **37**, 1157 (1980).
[20] R. Hide and P. J. Mason, Adv. Phys. **24**, 47 (1975).
[21] J. Guckenheimer and P. Holmes, *Nonlinear Oscillations, Dynamical Systems, and Bifurcations of Vector Fields* (Springer-Verlag, New York, 1983).
[22] J. R. Dormand and P. J. Prince, J. Comput. Appl. Math. **6**, 19 (1980).
[23] C. M. Strong, F.-F. Jin, and M. Ghil, J. Atmos. Sci. **50**, 2965 (1993).
[24] A. Brandstäter, J. Swift, H. L. Swinney, A. Wolf, J. D. Farmer, E. Jen, and P. J. Crutchfield, Phys. Rev. Lett. **51**, 1442 (1983).
[25] J. P. Gollub, S. V. Benson, and J. F. Steinman, Ann. N.Y. Acad. Sci. **357**, 22 (1980); M. Giglio, S. Musazzi, and V. Perini, Phys. Rev. Lett. **47**, 243 (1981); P. S. Linsay, *ibid.* **47**, 1349 (1981); W. Lauterborn and E. Crames, *ibid.* **47**, 1445 (1981).
[26] O. E. Rössler, Phys. Lett. A **57**, 397 (1976).
[27] E. N. Lorenz, *The Nature and Theory of the General Circulation of the Atmosphere* (World Meteorological Organization, Geneva, 1967).
[28] R. Benzi, A. Speranza, and A. Sutera, J. Atmos. Sci. **43**, 2962 (1986).
[29] E. R. Weeks, Y. Tian, J. S. Urbach, K. Ide, H. L. Swinney, and M. Ghil, Science **278**, 1598 (1997); Y. Tian, E. R. Weeks, K. Ide, J. S. Urbach, C. N. Baroud, M. Ghil, and H. L. Swinney, J. Fluid Mech. **438**, 129 (2001).
[30] B. J. Hoskins, in *Large-Scale Dynamical Processes in the Atmosphere*, edited by B. J. Hoskins and R. P. Pearce (Academic, New York, 1983); R. Vautard, B. Legras, and M. Déqué, J. Atmos. Sci. **45**, 2811 (1988); J. Marshall and F. Molteni, *ibid.* **50**, 1792 (1993).
[31] J. W. Kidson and I. G. Watterson, J. Atmos. Sci. **56**, 3859 (1999); S. Feldstein, J. Clim. **13**, 2356 (2000).
[32] H. Van Loon, in *Meteorology of the Southern Hemisphere*, edited by C. W. Newton (American Meterological Society, Boston, 1972); S. L. Marcus, M. Ghil, and J. O. Dickey, J. Atmos. Sci. **51**, 1431 (1994); **53**, 1993 (1996).
[33] D. J. Karoly, Tellus, Ser. A **42A**, 41 (1990); W. A. Robinson, *ibid.* **43A**, 295 (1991).
[34] D. W. J. Thompson and J. M. Wallace, Geophys. Res. Lett. **25**, 1297 (1998); J. Clim. **13**, 1000 (2000); J. M. Wallace, Q. J. R. Meteorol. Soc. **126**, 791 (2000).